The Journal of Chemical Physics

Desorption of CO from Ru(001) induced by near-infrared femtosecond laser pulses

Cite as: J. Chem. Phys. **112**, 9888 (2000); https://doi.org/10.1063/1.481626
Submitted: 06 August 1999 . Accepted: 13 March 2000 . Published Online: 31 May 2000

S. Funk, M. Bonn, D. N. Denzler, et al.


View Online


Export Citation

ARTICLES YOU MAY BE INTERESTED IN

Indication of non-thermal contribution to visible femtosecond laser-induced CO oxidation on Ru(0001)
The Journal of Chemical Physics **143**, 074701 (2015); https://doi.org/10.1063/1.4928646

Femtosecond laser induced associative desorption of H2 from Ru(0001): Comparison of "first principles" theory with experiment
The Journal of Chemical Physics **124**, 244702 (2006); https://doi.org/10.1063/1.2206588

Vibrational energy transfer of CO/Cu(100): Nonadiabatic vibration/electron coupling
The Journal of Chemical Physics **96**, 3950 (1992); https://doi.org/10.1063/1.461897

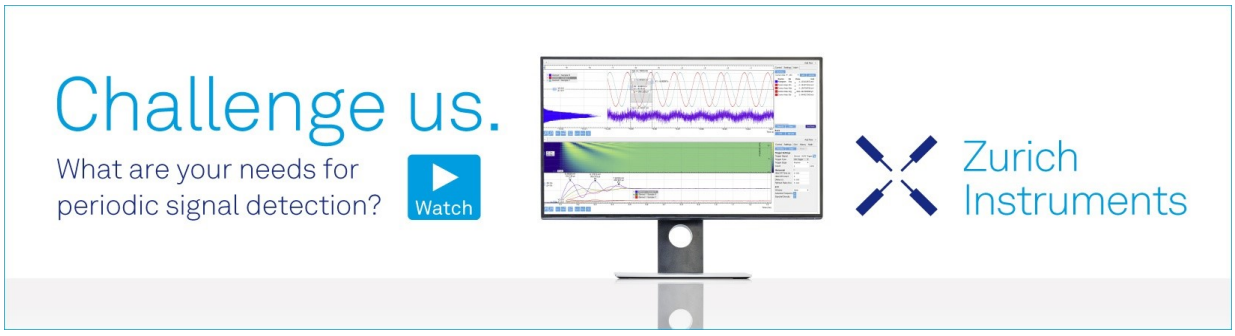

© 2000 American Institute of Physics.

AIP Publishing

Desorption of CO from Ru(001) induced by near-infrared femtosecond laser pulses

S. Funk, M. Bonn, D. N. Denzler, Ch. Hess, M. Wolf, and G. Ertl
Fritz-Haber-Institut der Max-Planck-Gesellschaft, Faradayweg 4-6, D-14195 Berlin, Germany

(Received 6 August 1999; accepted 13 March 2000)

Irradiation of a Ru(001) surface covered with CO using intense femtosecond laser pulses (800 nm, 130 fs) leads to desorption of CO with a nonlinear dependence of the yield on the absorbed fluence (100–380 J/m^2). Two-pulse correlation measurements reveal a response time of 20 ps (FWHM). The lack of an isotope effect together with the strong rise of the phonon temperature (2500 K) and the specific electronic structure of the adsorbate–substrate system strongly indicate that coupling to phonons is dominant. The experimental findings can be well reproduced within a friction-coupled heat bath model. Yet, pronounced dynamical cooling in desorption, found in the fluence-dependence of the translational energy, and in a non-Arrhenius behavior of the desorption probability reflect pronounced deviations from thermal equilibrium during desorption taking place on such a short time scale. © *2000 American Institute of Physics.* [S0021-9606(00)70122-X]

I. INTRODUCTION

In the traditional view of thermally activated surface reactions energy is transferred from the substrate to the adsorbate center-of-mass system solely via lattice phonons. However, surface reactions can also be triggered by coupling of the substrate electronic degrees of freedom to the adsorbate center-of-mass system.[1,2] Examples for this interaction include vibrational energy relaxation on metals,[3,4] charge transfer in gas–surface interactions,[5] atomic scale friction,[6] electron stimulated desorption,[7] and surface photochemistry.[8] The time scales of these processes lie in the pico- to femtosecond regime. Recently, considerable progress in ultrafast laser spectroscopy has laid the ground to elucidate the dynamics of the underlying elementary processes of charge and energy transfer directly in the time domain.[9,10]

In particular, a new class of nonequilibrium surface reactions has been established, in which the reaction is driven by the high density of excited substrate electrons induced by intense femtosecond laser pulses.[11] Examples of these processes include the desorption of small diatomic molecules from various metal[11–18] and oxide surfaces[19] and the photooxidation of CO with coadsorbed oxygen.[20–23] These systems share some common characteristics, namely (i) a highly nonlinear dependence of the desorption yield Y on the absorbed fluence F, ($Y \propto F^n$, with $3 \leqslant n \leqslant 8$ reported), (ii) an ultrafast response time (0.3–2 ps) in two-pulse correlation experiments,[12,21] (iii) highly vibrationally excited desorption products,[11,17,19] and (iv) branching ratios substantially differing from those found by excitation with ns-pulses or cw-light.[20,23,24] Some of these findings are incompatible with conventional thermal or photochemical mechanisms and it was demonstrated that the observations can be explained by direct electronic-vibrational coupling between the transient hot electron distribution in the substrate and the adsorbate degrees of freedom.

Two conceptionally different frameworks have been employed to describe fs-laser induced desorption. First, an adaptation of the Menzel–Gomer–Readhed model to the high electronic excitation conditions, the ''desorption induced by multiple electronic transitions'' (DIMET) was proposed.[13] The first step of this process is depicted in Fig. 1(a). After electronic excitation by a hot substrate electron, which is tunneling into a negative ion resonance, the adsorbate is accelerated towards its new equilibrium position. This results in an energy gain after the transition back to the ground state depending on the lifetime τ of the excited state. Due to the fs-laser induced high density of excited substrate electrons, a second excitation of the adsorbate may occur before vibrational relaxation is completed. Several of these cycles may result in an energy transfer, which is sufficient to overcome the barrier towards desorption. This causes a nonlinear dependence of the cross section on the excitation density in the substrate. Sophisticated trajectory calculations are necessary to calculate desorption probabilities within this model. In contrast to this diabatic picture of electronic transitions between different potential energy surfaces (PES), an alternative, adiabatic approach involves coupling between the electronic system and the adsorbate vibrational degrees of freedom within the electronic ground state of the adsorbate via electronic friction.[25,26] This frictional approach was originally introduced to describe the reverse process of the substrate-mediated vibrational heating we are interested in; The vibrational energy relaxation on metals via electron hole pair excitation in the substrate.[27–29] Brandbyge and coworkers have extended the frictional approach to comprise both DIMET and frictional coupling within a unified formalism.[30] The complexity of the DIMET process, which depends on the shape of the PES and the excited state lifetime, is reflected in this formalism by a friction strength which strongly varies with temperature and adsorbate–substrate distance for an energetically high lying resonance.

Also shown in Fig. 1(a) is the phonon-mediated excitation channel leading to desorption. Here scattering with sub-

 © 2000 American Institute of Physics

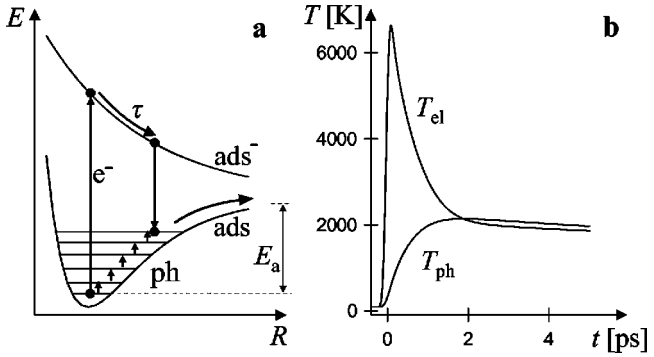

FIG. 1. (a) Electronically driven vs phonon-mediated vibrational heating of the adsorbate center-of-mass system. Shown are the potential energy surfaces of the electronic ground and excited state (ads and ads$^-$) as a function of the reaction coordinate R. (b) The nonequilibrium of electron (T_{el}) and phonon (T_{ph}) temperatures, caused by fs-laser excitation, allows us to discriminate between both contributions (calculated for Ru).

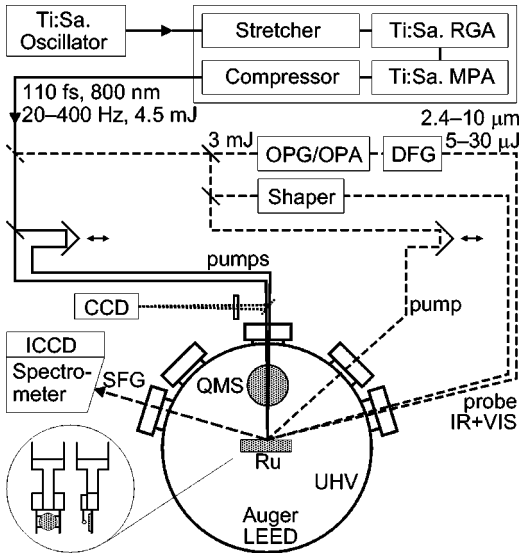

FIG. 2. Schematic diagram of the experimental setup combining high power femtosecond laser technology with ultrahigh vacuum. Solid lines indicate the beam pass for the desorption experiments while the dashed lines show the SFG-setup.

strate phonons vibrationally heats the adsorbate–substrate bond resulting in vibrational ladder climbing to overcome the activation energy E_a. The strength of this coupling has again been treated theoretically concerning its contribution to vibrational energy relaxation.[31] It is found to depend critically on the energy match between the surface phonons and the vibrational quanta along the reaction coordinate.

To investigate whether the mechanism of a surface reaction is either electronically driven or phonon-mediated vibrational heating, one can take advantage of the thermal nonequilibrium between the substrate electron and phonon system following fs-laser excitation. Figure 1(b) depicts the time-evolution of the electron (T_{el}) and phonon (T_{ph}) temperature at the surface as consequence of a fs-laser pulse centered at $t=0$ ps. Because of their low heat capacity, the electrons are heated up to temperatures far above the equilibrium melting point. Subsequently the electrons equilibrate with the phonons on a 2 ps time scale (on Ru) by electron–phonon scattering. This is considerably faster than diffusive heat-transfer into the bulk which takes tens of picoseconds [not shown in Fig. 1(b)]. Exciting the system with a second, delayed fs-laser pulse, the correlation function of the temperature transients is either narrow for the fast electronic slope or wide for the slow heat-transfer into the bulk. This is used in two-pulse correlation experiments, where the dependence of the desorption yield on the delay between the two pump pulses is a measure for the persistent time of the adsorbate excitation leading to desorption.

To model the outcome of such experiments, the phonon-mediated channel for vibrational heating and its electronic counterpart are incorporated in an empirical friction model[32] to calculate the adsorbate vibrational temperature of the reaction coordinate. Utilizing an Arrhenius type expression to quantitatively calculate the desorption rate, this model has been applied to fs-laser induced desorption of CO/Cu(001) by Struck and co-workers.[17]

In this article we present results on the desorption dynamics of CO from Ru(001) induced by intense femtosecond laser pulses (800 nm, 130 fs, 200–600 J/m^2 incident fluence). CO/Ru(001) was chosen because it is a well-characterized adsorption system on a transition metal surface.[33–37] The measured nonlinear fluence-dependence and the two-pulse correlation of the desorption yield are analyzed using the empirical friction model mentioned above. The strong electron–phonon coupling allows for heating the lattice to temperatures far above the equilibrium desorption temperature on a picosecond time scale. Since there is no electronic adsorbate resonance within reach of the transient hot electron distribution, this indicates a phonon-mediated desorption mechanism, which is consistent with the two-pulse correlation response that persists for tens of picoseconds. The yield of this laser-induced desorption by ultrafast heating is found to be inconsistent with the equilibrium Arrhenius behavior presupposed by the model. Also the average translational energy of the desorbing molecules is substantially lower than $2k_BT_S$ expected for the calculated surface temperature T_S. These features originate from the nonequilibrium conditions in ultrafast laser heating and are discussed within a detailed balance picture and on the basis of stochastical trajectory calculations by Tully.[38]

II. EXPERIMENT

Experiments were performed under combined use of an ultrahigh vacuum (UHV) chamber and a high power Ti:sapphire femtosecond laser system. Figure 2 schematically depicts the experimental setup.

The laser system consists of an Ar^+-laser (Coherent, Innova I-425) pumped Ti:sapphire oscillator (MIRA 9000), which is taken as a seed for a chirped-pulse amplification system (Quantronix, TitanII),[39] consisting of two Nd:YLF pump lasers, a stretcher, a regenerative and a multipass amplifier, and a compressor. After being stretched to 200 ps the pulses are amplified to 300 μJ in the regenerative stage, pumped by 6 mJ of frequency-doubled Nd:YLF output. A pulse picker is used to clean the RGA output from pre- and postpulses before it is send through a two-stage Ti:sapphire multipass amplifier, which is pumped by two frequency-

doubled Nd:YLF lasers with 29 mJ in total. After pulse-compression to 110 fs (FWHM), the system typically provides 800 nm pulses of 4.5 mJ pulse energy at a repetition rate of 400 Hz. The pulse picker allows for adjusting the repetition rate down to 20 Hz.

The sample is mounted in an UHV chamber with a base pressure of 2×10^{-10} mbar. It is fixed between a pair of tantalum wires, which are welded to tungsten posts mounted to the copper head of a liquid nitrogen Dewar. This way the sample can be cooled down to 95 K. Heating is provided alternatively by electron bombardment from the backside of the crystal or by resistive heating through the tantalum wires. A NiCr–Ni thermocouple is used to measure the sample temperature up to 1530 K. A quadrupole mass spectrometer (Balzers QMS421) is mounted through the bottom of the chamber in order to allow optical access to the sample through a cross beam ion source in line of sight of the QMS (see Fig. 2). Thermal desorption spectroscopy (TDS), along with low energy electron diffraction (LEED) and Auger electron spectroscopy (AES), both utilizing a retractable electron optics (VSI ErLEED), are employed as surface probes. Adsorbates can be dosed to the sample either directly through a retractable pinhole doser (5 μm orifice) or via the background pressure using a leak valve. A gas handling system provides control over various gases, e.g., of different isotopic composition. The UHV chamber is mounted in a circular cut of the laser table to enable stable and easy laser beam alignment.

For the desorption measurements the total output of the 800 nm amplifier is send unfocused or slightly focused through a MgF_2 window into the UHV chamber to irradiate the sample under normal incidence (solid lines in Fig. 2). The pulse energy and hence the fluence can be varied by changing the pump power of one of the Nd:YLF lasers. Because of the high incident fluences of up to 600 J/m^2 the beam profile gets distorted by self-focusing in the entrance window. To account for the resulting changes in the applied fluence, the profile is recorded at a position equivalent to the sample by a CCD camera after having passed a reference MgF_2 window; both windows were tested to cause similar self-focusing. A precise determination of the beam profile is necessary for the yield-weighing procedure described below. For the two-pulse correlation measurements the beam is split in two parts of equal energy, one of them passing a computer controlled delay line and a polarization flipper to minimize interference effects when both pulses are overlapped in space and time on the sample under a skew angle of 30″.

Reaction products are detected by the mass spectrometer after a 25–50 mm flight path along the surface normal. The QMS can be operated in a single molecule counting mode, using a multichannel scaler (SRS SR430) as counter, or in a current mode, requiring gated integration electronics (SRS SR250). Depending on the signal intensity, the favored detection method was chosen to achieve optimum signal to noise ratio while simultaneously avoiding saturation effects in the detection process. Time-of-flight spectra are recorded by measuring the time difference between the laser trigger and the arrival of the molecules at the QMS ionizer with the multichannel scaler.

The Ru(001) single crystal surface was cleaned by dosing oxygen and subsequently heating to 1500 K to oxidize and desorb carbon contamination.[40] Only when highly contaminated, Ar^+-sputtering (3 kV) at 1000 K and annealing for 10 min at 1500 K in a 2×10^{-7} mbar oxygen atmosphere was necessary. Care was taken to desorb all the oxygen from the surface prior to adsorption of CO. The surface quality and cleanliness was judged by TDS, only during the initial cleaning procedure LEED and AES were utilized.

Desorption experiments are performed under steady state conditions by dosing the sample continuously in a CO background of typically 2×10^{-8} mbar. The coverage is set by adjusting the surface temperature; 100–200 K are used for saturation coverage (0.68 monolayer, 1 ML $=1.58\times10^{15}$ cm^{-2}), whereas 430 K yields the $(\sqrt{3}\times\sqrt{3})R30°$ coverage (0.33 ML, further referred to as $\sqrt{3}$-coverage).[33] After opening a shutter, the surface is irradiated by a sequence of laser pulses that depletes the coverage; we report the first shot yield which is obtained from a fit to the total single shot yield as a function of laser shots. In between experiments a pause of typically 120 s allows the sample to be redosed via the background.

Also shown in Fig. 2 is the optical setup for time-resolved surface vibrational spectroscopy. The goal of these experiments is to monitor changes of the intramolecular C–O stretch mode during the desorption process directly in the time domain. We employ a scheme for sum-frequency generation (SFG), utilizing a broadband fs-infrared and a narrowband upconversion pulse.[41] SFG as $\chi^{(2)}$-process is interface sensitive, thus allowing for vibrational spectroscopy with (sub-)monolayer sensitivity. Using fs-pulsed IR-light combines two effects. First, because of the broad spectrum of fs-pulses, the complete spectral region of interest is covered without tuning the IR frequency. Using multichannel detection a complete spectrum can be obtained by one shot. The spectral resolution is determined by the narrowband upconversion pulse. Secondly, fs-pulsed operation allows SFG to be utilized as a probe in an ultrafast detection scheme.

The principle setup for the SFG experiments is indicated by the dashed lines in Fig. 2. To generate the broadband fs-IR pulses we use 3 mJ of the 800 nm amplifier output to pump a TOPAS (''traveling-wave optical parametric amplifier of superfluorescence,'' Light Conversion Ltd.) for optical parametrical generation (OPG) and two-pass amplification (OPA) of signal and idler in a single β-barium borate (BBO) crystal.[42] For tuning, the phase matching angle and a grating are adjusted to select and amplify only the desired wavelength from the super-fluorescence continuum. Subsequently the difference frequency between signal and idler is generated in an $AgGaS_2$ crystal. This provides a laser source for IR pulses of typically 130 fs duration that are tunable in the range of 2.4–10 μm with a pulse energy of 5–30 μJ, depending on the IR wavelength. The narrowband upconversion pulse of typically 5 μJ pulse energy is generated by spectrally shaping a portion of the amplifier output. The IR pulse is sent into the UHV chamber to irradiate the sample under grazing incidence to achieve maximum IR-induced polarization of the adsorbate layer. Here the IR pulse is overlapped in space and time with the upconversion pulse. The

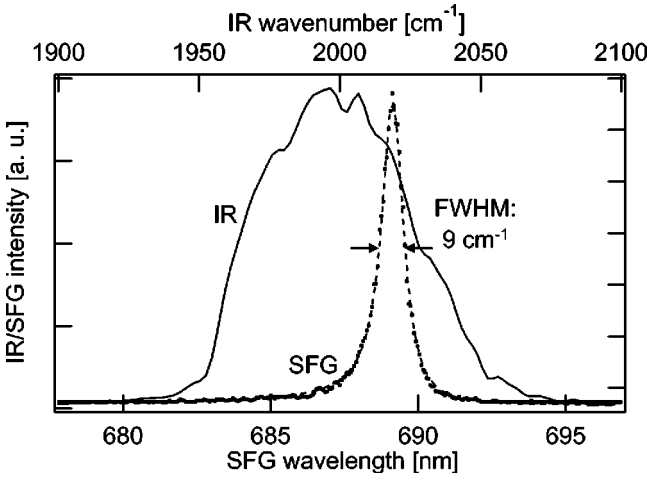

FIG. 3. SFG-spectrum of the internal stretch mode of CO adsorbed on Ru(001) taken at $\sqrt{3}$-coverage (200 K). The narrow band (5 cm^{-1}) upconverting pulse of 783 nm wavelength determines the spectral resolution.

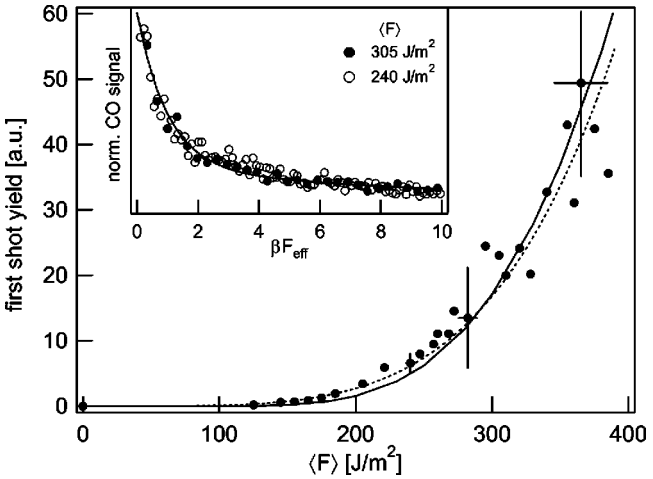

FIG. 4. Dependence of the CO desorption yield on the absorbed yield-weighted laser fluence $\langle F\rangle$ at a surface temperature of 200 K for saturation coverage (0.68 ML). Incident fluences range from 200 to 600 J/m^2. The dashed line shows the parameterization by a power-law $\langle F\rangle^n$ with $n=4.5$, the solid line is a fit according to the friction-model described in Sec. IV. The inset depicts the depletion of the surface coverage after multiple-pulse excitation for two different fluences. Both data sets are fitted to the same double exponential decay with 80% of the initial amplitude being described by the faster channel yielding a cross section of $\sigma_{\text{eff}}=1.7\times10^{-18}\,\text{cm}^2$ at $\langle F\rangle=305\,\text{J/m}^2$ (data normalized for clarity).

resulting SFG signal is spatially filtered by apertures and spectrally cleaned by shortwave-pass filters. After passing through an imaging spectrograph it is detected with photomultiplier sensitivity by an intensified and gated CCD camera to record the complete spectrum simultaneously. Figure 3 shows a first result of this SFG scheme for CO/Ru(001) at $\sqrt{3}$-coverage. Only that part of the broadband-IR pulse, which is resonant with the C–O stretch mode, is efficiently upconverted to the visible by the narrowband pulse of 783 nm wavelength. The measured Lorentzian linewidth of 9 cm^{-1} (FWHM) includes the spectral width of the upconversion pulse of 5 cm^{-1}. For time-resolved SFG-spectroscopy another portion of the 800 nm amplifier output can be used to initiate a reaction which is subsequently monitored by a time-delayed SFG-probe to obtain transient vibrational spectra.[43]

III. RESULTS

Irradiation of CO adsorbed on Ru(001) with intense 800 nm 130 fs laser pulses leads to desorption of molecular CO; no indication for dissociation was found. The dependence of the desorption yield on the laser fluence for saturation coverage (0.68 ML) is depicted in Fig. 4. The measured pulse energy and beam profile are used to calculate the yield-weighted absorbed fluence $\langle F\rangle$ for each measurement (reflectivity $R=0.61$). In order to do this, the fluence dependence of the yield Y is parameterized by a power-law $Y\propto F^n$. The fluence and the resulting yield of each camera pixel i enter a weighting procedure $\langle F\rangle=\Sigma Y_i F_i/\Sigma Y_i=\Sigma F_i^{n+1}/\Sigma F_i^n$, where n is fitted to the data in a self-consistent manner.[17] This is done to compensate for changes in the beam profile when the fluence is adjusted. The experiment yields a power law of $n=4.5\pm0.5$, shown as dashed line in Fig. 4.

The cross section for desorption can be evaluated from the depletion of the coverage after multiple-pulse excitation which is shown in the inset of Fig. 4. In case of a linear dependence of the yield on the fluence the coverage after the jth laser shot decays following $\theta_j=\theta_0\exp[-\sigma F(j)]$, where $F(j)=\Sigma_{i=1}^{j}F_i$ is the accumulated incident fluence, summed over the number of laser shots (analogously the amount of accumulated incident photons could be used). In the case of a nonlinear fluence-dependence the equation describing the depletion of the coverage can be generalized to $\theta_j=\theta_0\times\exp[-\beta F_{\text{eff}}(j)]$.[15] Here the effective accumulated incident fluence $F_{\text{eff}}(j)$ is defined as $F_{\text{eff}}(j)=\Sigma_{i=1}^{j}F_i^n$, where n is the exponent of the power-law (βF_{eff} is used as the ordinate in the inset of Fig. 4). In doing this the depletion curves of all fluences can be fitted by the same β, provided that the power-law gives a good description of the fluence-dependence. In Fig. 4 this is shown for two different fluences confirming the power law of $n=4.5$. The effective cross section is then defined as $\sigma_{\text{eff}}=\beta\Sigma F_i^n/\Sigma F_i$ which simplifies to $\sigma_{\text{eff}}=\beta F^{n-1}$ for summation over pulses of identical fluence. Hence, σ_{eff} is dependent on the fluence and, for pulses of $\langle F\rangle=305\,\text{J/m}^2$, it is determined to be $\sigma_{\text{eff}}=1.7\times10^{-18}\,\text{cm}^2$, in agreement with the value obtained assuming a linear dependence on the fluence. The desorption probability per pulse at this fluence is $P_{\text{des}}=\sigma_{\text{eff}}F=0.2$. This high desorption probability is consistent with the results of scan experiments. Here, after having scanned the whole surface with the desorption laser, we determined the desorbed fraction by the reduced intensity in TDS to be roughly consistent with P_{des}. We can therefore conclude that the CO desorption signal does not arise from minority species. It should be mentioned that for fluences higher than $\langle F\rangle\approx350\,\text{J/m}^2$, given the Gaussian shaped spatial pulse profile, saturation of the desorption ($P_{\text{des}}=1$) during a single pulse in its spatial center can not be excluded. Saturation may not be apparent from the fluence-dependence for pulse profiles differing from a flat-top.

As mentioned in the Introduction, insight into the dynamics of the excitation process can be obtained from two-pulse correlation measurements. In these experiments, fol-

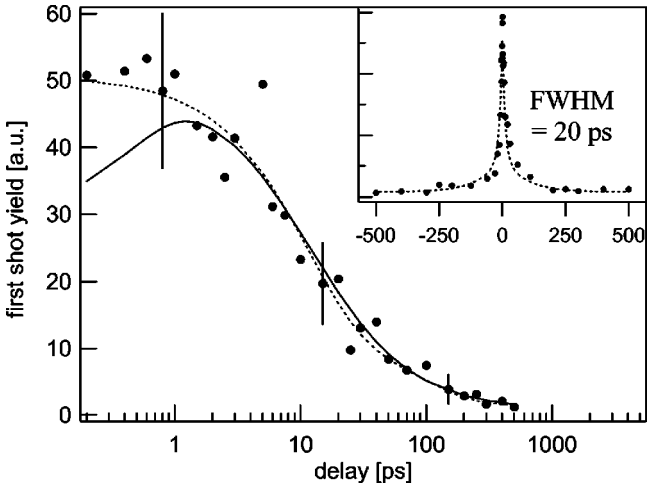

FIG. 5. Femtosecond two-pulse correlation of CO desorbing from Ru(001) at a surface temperature of 200 K (0.68 ML), indicating a time response of 20 ps (FWHM). The dashed line is a guide to the eye, the solid line reflects the result of friction-model calculations described in Sec. IV (note the logarithmic scale of the time-axis in the main graph).

lowing a pump–pump scheme of ultrafast detection, the time-integrated yield is measured as a function of the delay between the pump pulses, leading to a time resolution which is limited only by the pulse duration. Results for the saturation coverage [0.68 ML CO/Ru(001)] are shown in Fig. 5, indicating a time response of 20 ps (FWHM). The total absorbed fluence of $\langle F\rangle = 250\ \mathrm{J/m^2}$ is the sum of both pump pulses which have a fluence ratio of 52/48; negative delays indicate that the stronger pulse precedes. It should be noted, that despite our efforts to minimize interference between the two pump pulses by cross polarizing them, intensity modulations of ~10% were inevitable, giving rise to an additional systematic error for delays within the autocorrelation width.

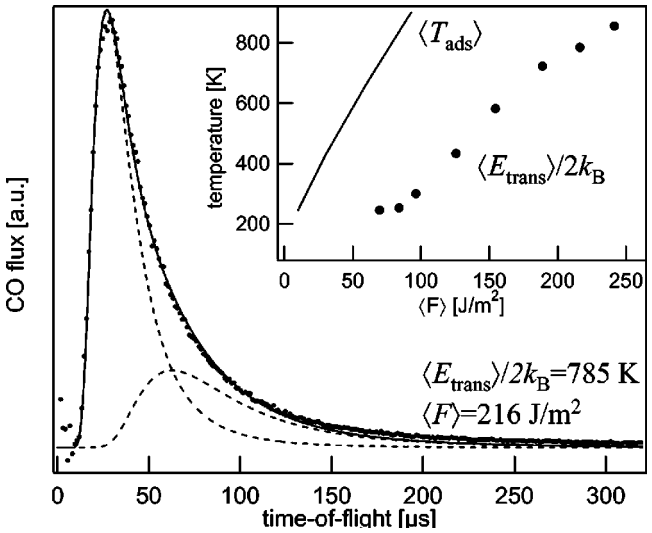

FIG. 6. Time-of-flight distribution of CO desorbing from Ru(001) after irradiation with 800 nm fs-laser pulses. The mean energy is calculated from a two-component modified Maxwell–Boltzmann fit and its dependence on the absorbed fluence is shown as circles in the inset (100 K initial sample temperature). The solid line represents the adsorbate temperature T_{ads} during the desorption to visualize the pronounced dynamical cooling effect discussed in Sec. V.

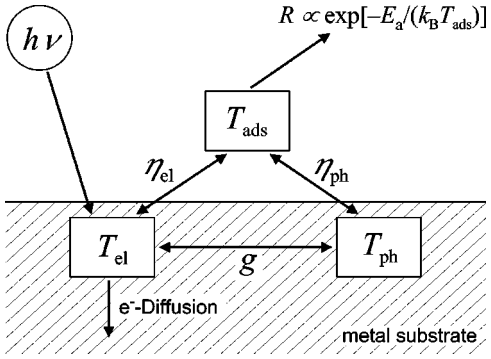

FIG. 7. Schematic representation of the energy flow in femtosecond laser-induced desorption assuming frictional coupling of the electron and phonon heat baths to the adsorbate degree of freedom.

Two-pulse correlation measurements of the $\sqrt{3}$-coverage yield a time response of 19 ps (FWHM, not shown in the figure). The ratio of the desorption probability per pulse between saturation and $\sqrt{3}$-coverage at the same absorbed fluence of $\langle F\rangle = 250\ \mathrm{J/m^2}$ is $P_{\mathrm{des}}(\mathrm{sat})/P_{\mathrm{des}}(\sqrt{3}) = 1.9 \pm 0.6$.

To characterize the energy release into the desorbing products we have measured the translational energy of the CO desorbed along the surface normal. Figure 6 shows an exemplary time-of-flight spectrum to illustrate the evaluation procedure where the spectra are fitted by two modified Maxwell–Boltzmann distributions. The necessity to use more than one component reflects the fact that, due to the Gaussian spatial pulse profile, the signal is an integral over a whole range of fluences; no further meaning is attributed to the two components of the fit. The flux-weighted average translational energy is calculated by analyzing the momenta of the resulting distribution.[44] As can be seen from the inset of Fig. 6, varying the absorbed fluence in the range of 70–240 J/m^2 leads to pronounced changes of the translational temperature $\langle E_{\mathrm{trans}}\rangle/2k_B$ between 250 and 850 K. All time-of-flight data were taken from saturation coverage at 100 K sample temperature.

In isotope exchange experiments, where the surface is covered with a 50/50-mixture of $^{12}C^{16}O$ and $^{13}C^{18}O$, no isotope effect was found in the composition of the CO desorption.

IV. MODELING

Femtosecond laser-induced desorption can be described by coupled heat baths for the electron, phonon, and adsorbate degrees of freedom, each characterized by its own temperature.[17,26,32] Figure 7 illustrates the flow of energy following fs-laser excitation within this model. The dynamics of the reaction are described by frictional coupling resulting in a delayed energy transfer between the electron, phonon, and adsorbate subsystem. The reaction rate is calculated by an Arrhenius expression. We refer to this model as the empirical friction model.

Initially, absorption of photons in the substrate ($h\nu$) creates a nonequilibrium electron–hole pair distribution which thermalizes by rapid electron–electron scattering. The electronic system can subsequently be described by an electron temperature T_{el}. Time-resolved experiments on gold at low

TABLE I. Thermodynamical and optical properties of Ruthenium used in the calculations of the two-temperature model.

Electron specific heat γ	400	$J\,m^{-3}\,K^{-2}$
Electron heat conductivity κ_0 (300 K)	117	$W\,m^{-1}\,K^{-1}$
Electron–Phonon coupling constant g	1.85×10^{18}	$W\,m^{-3}\,K^{-1}$
Debye temperature Θ_D	600	K
Atom density n	7.4×10^{28}	m^{-3}
Optical penetration depth λ (800 nm)	16.2×10^{-9}	m

excitation densities ($\Delta T_{el}\approx 100$ K) have shown that this thermalization occurs on a time scale of several hundreds of femtoseconds but becomes even faster at higher fluences.[45,46] In our experiments on Ru typical excitation conditions lead to a transient rise of electron temperature of $\Delta T_{el}\approx 3000-7000$ K. Therefore, and by taking into account the shorter electron–electron scattering time, in Ru the electrons thermalize while the pulse is absorbed.

The hot electron gas relaxes by electron–phonon coupling to the lattice phonons (T_{ph}) and by heat diffusion into the bulk.[47,48] The time evolution of the electron and lattice temperature (T_{el} and T_{ph}) can be evaluated using the two-temperature model of Anisimov,[49]

$$C_{el}\frac{\partial}{\partial t}T_{el}=\nabla_z\kappa\nabla_z T_{el}-g(T_{el}-T_{ph})+S(z,t), \tag{1}$$

$$C_{ph}\frac{\partial}{\partial t}T_{ph}=g(T_{el}-T_{ph}), \tag{2}$$

where $C_{el}=\gamma T_{el}$ and C_{ph} are the electron and lattice heat capacities, with the electron specific heat γ. κ and g refer to the thermal conductivity and the electron–phonon coupling constant, respectively. Lateral diffusion can be neglected since the beam diameter is much larger than the electron diffusion length, reducing the dimensionality to the distance z along the surface normal. The source term is given by

$$S(z,t)=(1-R)I(t)\lambda^{-1}e^{-z/\lambda} \tag{3}$$

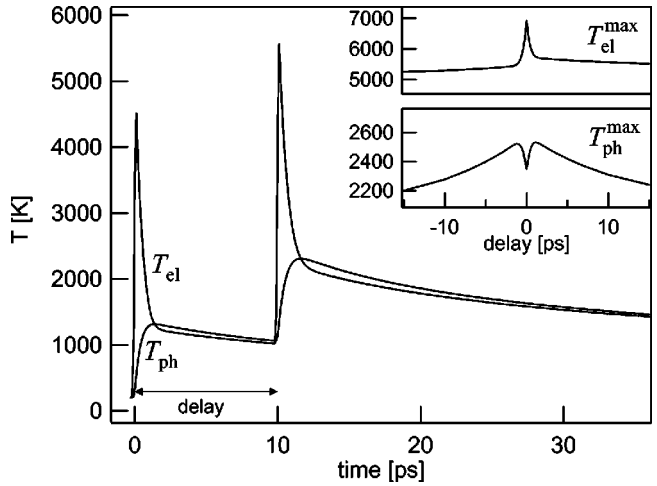

FIG. 8. Two-temperature model calculations reflecting the experimental conditions of Fig. 5. The inset shows the maximal electron and phonon temperatures at the surface as a function of the delay between the two pulses.

with the optical penetration depth λ, the substrate reflectivity R, and the temporal profile of the laser intensity $I(t)$ which is taken as Gaussian. The temperature dependence of the thermal conductivity is described by $\kappa=\kappa_0(T_{el}/T_{ph})$.[50] The Debye model provides an expression for the lattice heat capacity C_{ph},[51]

$$C_{ph}=9nk_B\left(\frac{T_{ph}}{\Theta_D}\right)^3\int_0^{\Theta_D/T_{ph}}dx\,\frac{x^4e^x}{(e^x-1)^2}, \tag{4}$$

where Θ_D is the Debye temperature and n the atom density. The relevant parameters for ruthenium are listed in Table I.

Figure 8 shows the prediction of the two-temperature model for the electron and phonon surface temperatures, given our experimental conditions for two-pulse excitation ($\langle F_1\rangle=120\,J/m^2$, $\langle F_2\rangle=130\,J/m^2$, 110 fs pulse duration, negative delays indicate the stronger pulse preceding the weaker pulse). Because of its low heat capacity, the electronic system is heated to several thousands of Kelvin before equilibrating with the lattice vibrational modes by electron–phonon coupling within 2 ps. For delays shorter than that, the second pulse drives the system even further from equilibrium, resulting in a 30% spike of the maximum electronic temperature T_{el}^{max} shown in the inset of Fig. 5. Both the electrons and phonons cool down by heat diffusion into the bulk via the electrons on a 55 ps time scale ($1/e$), leading to a time response of T_{ph}^{max} as depicted in the inset of Fig. 5. Consequently in a two-pulse correlation experiment, the response time for electronically driven processes is expected to be on the order of a few ps whereas phonon-mediated processes are expected to be an order of magnitude slower.

Note the 10% dip in the maximum phonon temperature around zero delay which has been ignored previously.[17] It is a result of the competition between electron–phonon coupling and hot electron transport into the bulk or, more precisely, of the nonlinearity of the diffusion term $\nabla_z\kappa_0(T_{el}/T_{ph})\nabla_z T_{el}$ with respect to T_{el}. Higher electronic temperatures imply a more effective heat transport into the bulk resulting in a lower phonon temperature at the surface. Thus, the spike in T_{el}^{max} causes the dip in T_{ph}^{max}. Using transient reflectivity measurements (pump–pump-reflectivity probe) this effect has been observed on various metal surfaces including ruthenium confirming the validity of the two-temperature model in a convincing way.[52]

Energy transfer from the electron and phonon system to the adsorbate is described by frictional coupling of the heat baths to an harmonic oscillator representing the adsorbate. A master equation approach yields[26,32]

$$\frac{d}{dt}U_{ads}=\eta_{el}(U_{el}-U_{ads})+\eta_{ph}(U_{ph}-U_{ads}), \tag{5}$$

where the energy U_x of the oscillator in a heat bath of the temperature T_x can be calculated as

$$U_x=\frac{h\nu_{ads}}{e^{h\nu_{ads}/(k_BT_x)}-1}. \tag{6}$$

Here ν_{ads} refers to the frequency of the vibration along the reaction coordinate, which in our case is assumed to be the low-frequency CO–Ru vibration ($\nu_{ads}=1.3\times10^{13}\,s^{-1}$).[36]

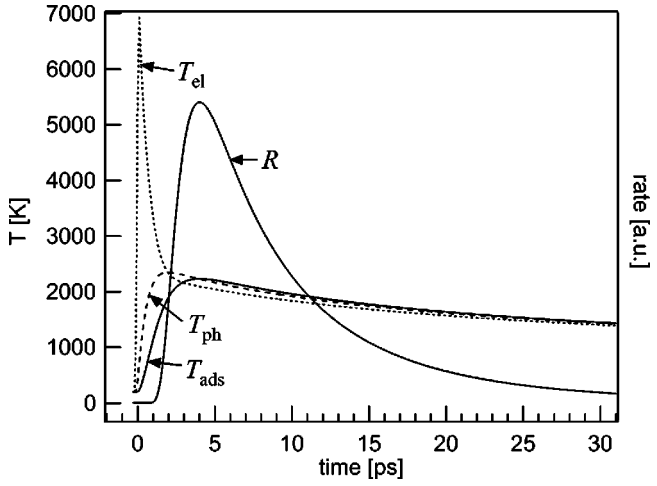

FIG. 9. Temperature transients of the coupled heat baths and the resulting desorption rate calculated with $\tau_{ph}=1$ ps and no coupling to the electrons, given the experimental conditions of Fig. 5 (zero delay). In an electronic scenario the adsorbate temperature T_{ads} would follow T_{el} more closely leading to a higher rate which peaks earlier and is more focused in time.

The friction coefficients can be understood as inverse energy relaxation times ($\eta=1/\tau$) of the adsorbate–substrate vibrational mode and have been used to explain vibrational excitation and relaxation.[26,32] In this respect they are connected to the energy lifetime and therefore the IR-linewidth of the corresponding vibration.

After determining the adsorbate temperature, the desorption rate is calculated by an Arrhenius type expression assuming first order kinetics,

$$R=-\frac{d}{dt}\theta=\theta k_0 e^{-E_a/(k_B T_{ads})}. \tag{7}$$

Time-integration gives the desorption probability $P_{des}=\int dt R$, which is fitted to the experimental data. Figure 9 shows the transient temperatures and the desorption rate for a set of parameters describing a phonon-mediated scenario used in the following discussion ($\tau_{ph}=1$ ps, infinite τ_{el}).

An alternative model, which describes only electronic friction has been proposed by Brandbyge and co-workers.[30] Here the electronic friction couples Langevin noise of the electron heat bath (T_{el}) into the adsorbate center-of-mass system (T_{ads}). Similar approaches have been used to describe the inverse process, the vibrational energy relaxation, where the adsorbate can be considered in a Brownian motion, dissipating energy to the electron heat bath. T_{ads} is calculated from T_{el} according to

$$\frac{d}{dt}T_{ads}=\eta(T_{el}-T_{ads}). \tag{8}$$

The desorption probability is again governed by a Boltzmann factor

$$P_{des}=E_a\int_0^\infty dt\,\frac{\eta}{T_{ads}}e^{-E_a/(k_B T_{ads})}, \tag{9}$$

but in contrast to Eq. (7) the friction coefficient η and T_{ads} also enter the pre-exponential. Taking into account the mass dependence of the friction coefficient $\eta\propto 1/M$ this model will predict an isotope effect in contrast to the empirical friction model discussed above. We employed this model in its low excitation limit, where the friction coefficient is independent of the temperature and the surface–adsorbate distance ($\eta=$const.), to calculate the isotope effect for a scenario where desorption is driven exclusively by coupling to hot electrons.

V. DISCUSSION

To extract information about the excitation mechanism the two-pulse correlation and the fluence dependence are fitted simultaneously utilizing the empirical friction model. We first discuss the limits of pure electronic and pure phonon coupling to the adsorbate, although generally both mechanisms can be operative simultaneously in fs-laser induced reactions.

In the phonon scenario (infinite τ_{el}), good fits can be obtained with τ_{ph} ranging from 0.5 to 3 ps. Figures 4 and 5 show the best fit with $\tau_{ph}=1$ ps; the transient adsorbate temperature T_{ads} and the resulting desorption rate R are shown in Fig. 9. The two-pulse correlation width of 20 ps (FWHM) for saturation coverage and 19 ps (FWHM) for $\sqrt{3}$-coverage are well reproduced taking into account the different activation energies ($E_a=1.2$ and 1.65 eV, respectively, obtained from TDS data[33]).

One prediction of the model is not found in the data; the 20%-dip at zero delay (see Fig. 5), which is the consequence of the 10%-dip in T_{ph}^{max}, amplified by the Boltzmann-factor in Eq. (7). The inset of Fig. 8 suggests the possibility to compensate for the dip in T_{ph} by adding adequate coupling to the electrons. However, this would require $\tau_{el}\leqslant 0.5$ ps, but with this parameter the calculated power-law exponent of the fluence dependence is much to small. Correspondingly too much signal in the wings of the two-pulse correlation is predicted. The dip is a prediction of the friction model for systems with slow coupling to electrons or dominant coupling to phonons, like CO/Ru(001) and CO/Cu(100).[17] The absence of the dip in the two-pulse correlation measurements for these systems questions the validity of the model. Yet, systematic errors in the experiments due to interference effects around zero delay hinder a final conclusion on this issue.

Pure electronic scenarios (infinite τ_{ph}), however, also lead to fair agreement with the desorption data for CO/Ru for 2 ps$\leqslant\tau_{el}\leqslant$4 ps. For $\tau_{el}=2$ ps the adsorbate temperature T_{ads} will follow T_{ph} (not shown in Fig. 9). The outcome of such a calculation is almost identical to the phonon scenario plotted in Figs. 4 and 5. This ambiguity lies inherently in the model for electronic coupling times τ_{el} longer than the electron–phonon equilibration time $\tau_{el-ph}=C_{ph}/g$ (=1.6 ps for Ru at ambient temperature).[32] Therefore additional arguments are required to decide on either mechanism. These will be provided by discussing the electronic structure of the adsorbate system and the absolute temperatures reached during the desorption process and by comparing these properties to the CO/Cu(100) system. For the latter system the friction model was used to deduce an electron dominated excitation process out of a two-pulse correlation width of ~3 ps (FWHM) by Struck and co-workers.[17]

Let us first consider the adsorbate electron affinity level, responsible for electronic interaction with substrate electrons, which is assumed to be the CO $2\pi^*$-orbital. By inverse photoemission it is found to be located 4.9 eV above the Fermi energy (E_F) for the saturation coverage of CO/Ru(001),[53] in contrast to CO/Cu(100),[54] where a doublet resonance is found at 2.4 and 3.9 eV above E_F. Given the experimental conditions, the electronic temperatures reach values of $T_{\mathrm{el}}^{\max} \approx 3400$ K and 6900 K for CO/Cu and CO/Ru, respectively. The resulting electron density at the $2\pi^*$-level thus is three orders of magnitude higher on Cu than on Ru. In addition, according to the Fermi-liquid theory, electrons closer to E_F have longer lifetimes and hence a longer mean free path: they can scatter into the affinity level from deeper within the bulk. Therefore the total amount of available electrons at the CO-$2\pi^*$ is about four orders of magnitude higher on Cu than on Ru. Quantitatively, according to this rough estimate, on Ru there are only $\sim 10^{-3}$ electrons available per adsorbate molecule, which energetically could populate the adsorbate affinity level. This would not be sufficient to cause the measured desorption probability of $P_{\mathrm{des}} = 0.2$ at $\langle F \rangle = 305\ \mathrm{J/m^2}$.

Comparing the temperatures reached during the desorption reveals another difference between Ru and Cu. In Ru an absorbed fluence which is six times higher than in Cu causes the electrons to reach a temperature only two times higher than in Cu. Since the electron–phonon coupling is more efficient in Ru, the energy is transferred to the lattice before the electrons heat up to temperatures like in Cu. Thus, the ratio between the maximum phonon and electron temperatures $T_{\mathrm{ph}}^{\max}/T_{\mathrm{el}}^{\max} \approx 0.3$ is higher for Ru, compared to Cu were it is only ≈ 0.1. In our experiments on Ru, the phonons reach a temperature of $T_{\mathrm{ph}}^{\max} \approx 2500$ K, whereas in the experiments on Cu only ≈ 440 K was reached. Quantitatively, the difference in lattice temperatures leads to a Boltzmann-factor in Eq. (7) five orders of magnitude higher for CO/Ru than for CO/Cu ($E_a = 1.2$ eV and 0.57 eV, respectively, given the experimental conditions).

The low density of electrons at the adsorbate affinity level and the high phonon temperatures strongly suggests that the phonon contribution is predominant for CO/Ru. This conclusion is encouraged by the theoretical findings of Persson,[31] which indicate that coupling to the phonons is effective in vibrational energy relaxation for modes with frequencies smaller than the Debye frequency of the metal $\nu_{\mathrm{ads}} < 2\,\nu_D$ ($\nu_D = 417\ \mathrm{cm^{-1}}$ for Ru, $\nu_{\mathrm{ads}} = 452\ \mathrm{cm^{-1}}$ for the CO–Ru stretch mode). Also the coupling is found to become increasingly efficient at higher temperatures. From IR absorption spectroscopy of the CO–Ru stretch mode a linewidth of 5 $\mathrm{cm^{-1}}$ is deduced,[36] which corresponds to a lower limit (neglecting pure dephasing) for the energy relaxation time of 1 ps at ambient temperature. This is consistent with the results of the friction model and even shorter coupling times may be rationalized by the high temperatures reached in the experiment.

The absence of an isotope effect on the desorption yield is a further argument against an electronic mechanism. As demonstrated for the oxidation of CO/Ru with coadsorbed atomic oxygen, where the electronically driven activation of the oxygen is the rate-determining step, an electronic mechanism lays the ground for a pronounced effect of isotopic substitution of the atomic oxygen.[23] This is caused by a stronger coupling of a lighter adsorbate to the electronic system due to a faster response to the driving fluctuating forces as described in the electronic friction model by Brandbyge and co-workers (see Sec. IV). For the desorption of CO from Ru this model predicts an isotope effect of $Y(^{28}\mathrm{(CO)})/Y(^{31}\mathrm{(CO)}) = 1.2$ for an electronic scenario. Since the magnitude of an isotope effect depends on the difference in η for different masses in relation to the steepness of the corresponding temperature slope, there should be only a small effect for phonon-driven processes.

All the arguments presented strongly favor coupling of the lattice phonons to the adsorbate motion as the dominant mechanism underlying desorption. We have shown that the friction model gives a good *qualitative* description of the experimental data, despite using only a few parameters; the friction coefficients η_{el} and η_{ph}, which are related to the coupling times $\eta = 1/\tau$ and are used to calculate the adsorbate temperature T_{ads}, the activation energy E_a and the pre-exponential factor k_0.

We will now discuss the ability of the model to *quantitatively* reproduce the desorption yield. To do so, we first take a closer look at the pre-exponential factor k_0 in Eq. (7), neglected so far. To achieve agreement of the model with the measured desorption probability for saturation coverage ($P_{\mathrm{des}} = 0.2$ at $\langle F \rangle = 305\ \mathrm{J/m^2}$), a value of $k_0 = 5 \times 10^{12}\ \mathrm{s^{-1}}$ is required, which is an order of magnitude smaller than the equilibrium value of $k_0 = 1 \times 10^{14}\ \mathrm{s^{-1}}$ found by TDS studies for the same coverage.[33] This deviation must be treated with some caution since the actual transient surface temperatures are not measured but calculated. Comparing the experimentally determined damage threshold for the fluence to the value which causes the lattice temperature to exceed the equilibrium melting point of Ru according to the model yields a rough estimate of the temperature uncertainty of 30%, corroborating the calculated temperatures. The value for k_0, deduced from the friction model, however, agrees fairly well with the frequency of the vibration along the reaction coordinate, which is only slightly coverage dependent, $\nu_{\mathrm{ads}} = 1.3 \times 10^{13}\ \mathrm{s^{-1}}$.[36] This suggests the interpretation of k_0 as attempt frequency. Another argument, which questions the use of the equilibrium k_0 to describe the desorption probabilities under fs-excitation, avoids the uncertainty in absolute temperatures by comparing the relative yield between saturation and $\sqrt{3}$-coverage. In TDS-studies a huge difference in k_0 of three orders of magnitude between the two coverages is found.[33] In the present case however, the experimentally observed difference in desorption probability can be explained simply by the different activation energies for the two coverages.

A further inconsistency with equilibrium behavior is found in the relatively low translational energy of the desorption products. Considering desorption of an adsorbate in thermal equilibrium with the surface, an average translational energy of $\langle E_{\mathrm{trans}} \rangle = 2k_BT$ is expected. As can be seen from the inset in Fig. 6, $\langle E_{\mathrm{trans}} \rangle$ is by a factor of 2–3 lower than the predicted rate-weighted adsorbate temperature

$\langle T_{ads} \rangle$ (solid line). Note that $\langle T_{ads} \rangle$ is only about 10% lower than $\langle T_{ph} \rangle$, indicating that the retarded energy transfer due to the finite coupling time τ_{ph} is only a minor effect. It should be pointed out out that because of the high desorption rate (about 0.1 ML in 10 ps) gas phase collisions lead to a focusing towards and acceleration along the surface normal,[55] the cooling effect is therefore even underestimated.

In conclusion significant deviations from the equilibrium behavior are found in fs-laser induced desorption of CO/Ru regarding the desorption yield and the translational energy. Similar indications for nonequilibrium conditions at high surface temperatures have been elaborated theoretically by Tully.[38] In the following we briefly review his key findings and discuss the consequences for fs-laser induced desorption. Tully considered a closed system, consisting of rare-gas atoms (Ar, Xe) which are in thermal equilibrium with a platinum surface before the system is suddenly evacuated. Classical trajectories in three dimensions were calculated stochastically to determine the sticking probability P_S as a function of the equilibrium gas and surface temperature. P_S is found to decrease with increasing surface temperature. Also $\langle E_{trans} \rangle / 2k_B T$ is found to be lower than one and to decrease with increasing temperature. Tully then proceeds to calculate the desorption rate from the sticking probability. The temperature dependence of this rate differs significantly from an Arrhenius behavior. This finding can be rationalized by considering the mean energy transfer upon each collision of the adsorbate with the surface to be less than $k_B T$. The relative energy transfer $\langle \Delta E \rangle / k_B T$ is less than unity and decreases with increasing temperature. This directly explains the experimentally observed translational cooling in desorption; The molecules in the high-energy tail of the Maxwell–Boltzmann distribution defined by the surface temperature are underrepresented resulting in a translational energy distribution below the surface temperature. Equilibration with the surface would require additional energy exchange by collisions with the surface, which do not occur due to rapid desorption. Thus the translational cooling is dynamical in origin. Also a desorption rate lower than expected from an Arrhenius behavior can be understood in this dynamical picture. The reduced efficiency of energy transfer implies that it takes longer at higher temperatures to establish a thermal distribution of the population of the levels near the top of the potential well. Thus, for a constant collision frequency the effective pre-exponential factor for the desorption rate decreases with rising temperatures. Additionally, depletion of the coverage due to desorption reduces the population of the levels near the top of the well, compared to a thermal distribution, which in turn affects the desorption rate. A desorption rate below the expectations for an Arrhenius behavior is again just what we observe in our experiments.

Another way of treating the translational cooling in desorption is provided by the principle of detailed balance. Here the desorption can be regarded as the inverse process of adsorption, linked by the sticking probability P_S. If molecules do not desorb with a certain translational energy, this implies, in a detailed balance picture, that molecules of that translational energy, coming from the gas phase, will not stick to the surface. This is because the excess energy can not be transferred to the substrate by a single collision, the molecule is repelled back to the gas phase. Thus translational cooling in desorption is equivalent to a dependence of sticking probability P_S on the incident kinetic energy, with P_S decreasing with increasing kinetic energy. This is indeed found in the trajectory calculations of Tully.

All dynamical effects discussed above also apply to the case of fs-laser excitation. The measurements on translational cooling in desorption therefore contain information about the dynamics of vibrational energy transfer leading to desorption. In principle this information can be extracted by applying detailed balance considerations.

VI. SUMMARY

Summarizing, we have characterized the excitation mechanism for the desorption of CO from the (001)-face of ruthenium induced by high intensity fs-laser pulses. Two-pulse correlation and fluence-dependence measurements are simultaneously fitted by an empirical friction model, which qualitatively reproduces the data. The remaining ambiguity in discerning between an electron- or phonon-mediated process, lying inherently in the model for electronic coupling times of the order of the electron–phonon thermalization time, is overcome by considering the absence of an electronic state within reach of the transient hot electron energy distribution. Because of the strong electron–phonon coupling also the lattice is heated up to a temperature close to the melting point. Though lasting only tens of picoseconds, but being far above the equilibrium desorption temperature, this temperature transient results in a desorption probability of nearly $P_{des} = 1$ in the phonon-mediated fs-laser induced desorption of CO/Ru(001).

Equilibrium rate constants are found to be inadequate to reproduce the measured desorption probabilities quantitatively. This, along with the pronounced translational cooling effect observed, reflects the dynamical nature of the process, taking place far from thermal equilibrium. This is despite the fact that vibrational heating is relatively slow in the CO/Ru system compared to electronically driven systems like CO/Cu(100), where equilibrium concepts are thus even more questionable. Further measurements, ideally including angular distributions, state-resolved studies and variation of the laser pulse duration, should help to obtain a more detailed picture of the desorption dynamics and to address fundamental questions about the validity of the temperature concept for the reaction coordinate and the dynamical effects that determine the desorption probability and the final state distributions.

ACKNOWLEDGMENTS

The authors would like to thank T. F. Heinz and H. Over for valuable comments and discussions. This work was supported in part by the Deutsche Forschungsgemeinschaft through SFB 450. M.B. thanks the European Commission for financial support through TMR Contract No. ERBFMBICT982971.

[1] R. R. Cavanagh, D. S. King, J. C. Stephenson, and T. F. Heinz, J. Phys. Chem. **97**, 786 (1993).
[2] C. T. Rettner, D. J. Auerbach, J. C. Tully, and A. W. Kleyn, J. Phys. Chem. **100**, 13021 (1996).
[3] P. Guyot-Sionnest, P. Dumas, Y. J. Chabal, and G. S. Higashi, Phys. Rev. Lett. **64**, 2156 (1990).
[4] J. D. Beckerle, R. R. Cavanagh, M. P. Casassa, E. J. Heilweil, and J. C. Stephenson, J. Chem. Phys. **95**, 5403 (1991).
[5] T. Greber, R. Grobecker, A. Morgante, A. Böttcher, and G. Ertl, Phys. Rev. Lett. **70**, 1331 (1993).
[6] B. N. J. Persson, *Sliding Friction: Physical Principles and Applications* (Springer, Berlin, 1998).
[7] R. D. Ramsier and J. T. Yates, Jr., Surf. Sci. Rep. **12**, 243 (1991).
[8] X.-L. Zhou, X.-Y. Zhu, and J. M. White, Surf. Sci. Rep. **13**, 73 (1991).
[9] *Laser Spectroscopy and Photochemistry on Metal Surfaces*, edited by H. L. Dai and W. Ho (World Scientific, Singapore, 1995), Vols. I and II.
[10] H. Petek and S. Ogawa, Prog. Surf. Sci. **56**, 239 (1998).
[11] J. A. Prybyla, T. F. Heinz, J. A. Misewich, M. M. T. Loy, and J. H. Glownia, Phys. Rev. Lett. **64**, 1537 (1990).
[12] F. Budde, T. F. Heinz, M. M. T. Loy, J. A. Misewich, F. d. Rougemont, and H. Zacharias, Phys. Rev. Lett. **66**, 3024 (1991).
[13] J. A. Misewich, T. F. Heinz, and D. M. Newns, Phys. Rev. Lett. **68**, 3737 (1992).
[14] J. A. Prybyla, H. W. K. Tom, and G. D. Aumiller, Phys. Rev. Lett. **68**, 503 (1992).
[15] F.-J. Kao, D. G. Busch, D. Cohen, D. Gomes da Costa, and W. Ho, Phys. Rev. Lett. **71**, 2094 (1993).
[16] J. A. Misewich, A. Kalamarides, T. F. Heinz, U. Höfer, and M. M. T. Loy, J. Chem. Phys. **100**, 736 (1994).
[17] L. M. Struck, L. J. Richter, A. Buntin, R. R. Cavanagh, and J. C. Stephenson, Phys. Rev. Lett. **77**, 4576 (1996).
[18] D. G. Busch and W. Ho, Phys. Rev. Lett. **77**, 1338 (1996).
[19] G. Eichorn, M. Richter, K. Al-Shamery, and H. Zacharias, Chem. Phys. Lett. **289**, 367 (1998).
[20] F.-J. Kao, D. G. Bush, D. Gomes da Costa, and W. Ho, Phys. Rev. Lett. **70**, 4098 (1993).
[21] S. Deliwala, R. J. Finlay, J. R. Goldman, T. H. Her, W. D. Mieher, and E. Mazur, Chem. Phys. Lett. **242**, 617 (1995).
[22] T.-H. Her, R. J. Finlay, C. Wu, and E. Mazur, J. Chem. Phys. **108**, 8595 (1998).
[23] M. Bonn, S. Funk, Ch. Hess, D. N. Denzler, C. Stampfl, M. Scheffler, M. Wolf, and G. Ertl, Science **285**, 1042 (1999).
[24] J. A. Misewich, S. Nakabayashi, P. Weigund, M. Wolf, and T. F. Heinz, Surf. Sci. **363**, 204 (1996).
[25] D. M. Newns, T. F. Heinz, and J. A. Misewich, Prog. Theor. Phys. Suppl. **106**, 411 (1991).
[26] F. Budde, T. F. Heinz, A. Kalamarides, M. M. T. Loy, and J. A. Misewich, Surf. Sci. **283**, 143 (1993).
[27] B. N. J. Persson and M. Persson, Solid State Commun. **36**, 175 (1980).
[28] J. C. Tully, M. Gomez, and M. Head-Gordon, J. Vac. Sci. Technol. A **11**, 1914 (1993).
[29] J. P. Culver, M. Li, Z.-J. Sun, R. M. Hochstrasser, and A. G. Yodh, Chem. Phys. **205**, 159 (1996).
[30] M. Brandbyge, P. Hedegård, T. F. Heinz, J. A. Misewich, and D. M. Newns, Phys. Rev. B **52**, 6042 (1995).
[31] B. N. J. Persson, J. Phys. C **17**, 4741 (1984).
[32] T. A. Germer, J. C. Stephenson, E. J. Heilweil, and R. R. Cavanagh, J. Chem. Phys. **101**, 1704 (1994).
[33] H. Pfnür, P. Feulner, and D. Menzel, J. Chem. Phys. **79**, 4613 (1983).
[34] H. Pfnür and D. Menzel, J. Chem. Phys. **79**, 2400 (1983).
[35] P. Jakob, Phys. Rev. Lett. **77**, 4229 (1996).
[36] P. Jakob, J. Chem. Phys. **108**, 503 (1998).
[37] J. Braun, K. L. Kostov, G. Witte, and C. Wöll, J. Chem. Phys. **106**, 8262 (1997).
[38] J. C. Tully, Surf. Sci. **111**, 461 (1981).
[39] Q. Fu, F. Seier, S. K. Gayen, and R. R. Alfano, Opt. Lett. **22**, 712 (1997).
[40] T. E. Madey, H. A. Engelhardt, and D. Menzel, Surf. Sci. **48**, 304 (1975).
[41] L. J. Richter, T. P. Petralli-Mallow, and J. C. Stephenson, Opt. Lett. **23**, 1594 (1998).
[42] R. Danielius, A. Piskarskas, A. Stabinis, G. P. Banfi, P. Di Trapani, and R. Righini, J. Opt. Soc. Am. B **10**, 2222 (1993).
[43] M. Bonn, Ch. Hess, S. Funk, J. M. Miners, B. N. J. Persson, M. Wolf, and G. Ertl, Phys. Rev. Lett. (in press).
[44] E. Hasselbrink, in *Laser Spectroscopy and Photochemistry on Metal Surfaces*, edited by H. L. Dai and W. Ho (World Scientific, Singapore, 1995), Vol. II, p. 685.
[45] W. S. Fann, R. Storz, H. W. K. Tom, and J. Bokor, Phys. Rev. B **46**, 13592 (1992).
[46] N. Del Fatti, R. Bouffanais, F. Vallée, and C. Flytzanis, Phys. Rev. Lett. **81**, 922 (1998).
[47] R. H. M. Groeneveld, R. Sprik, and A. Lagendijk, Phys. Rev. B **45**, 5079 (1992).
[48] T. Juhasz, H. E. Elsayed-Ali, G. O. Smith, C. Suárez, and W. E. Bron, Phys. Rev. B **48**, 15488 (1993).
[49] S. I. Anisimov, B. L. Kapeliovich, and T. L. Perel'man, Zh. Eksp. Teor. Fiz. **66**, 776 (1974) [Sov. Phys. JETP **39**, 375 (1974)].
[50] N. W. Ashcroft and N. D. Mermin, *Solid State Physics* (Saunders College, Philadelphia, 1988).
[51] C. Kittel, *Introduction to Solid State Physics* (Wiley, New York, 1996).
[52] M. Bonn, D. N. Denzler, S. Funk, M. Wolf, S. S. Wellershoff, and J. Hohlfeld, Phys. Rev. B **61**, 1101 (2000).
[53] C. Benndorf, E. Bertel, V. Dose, W. Jacob, N. Memmel, and J. Rogozik, Surf. Sci. **191**, 455 (1987).
[54] J. Rogozik, V. Dose, K. C. Prince, A. M. Bradshaw, P. S. Bagus, K. Hermann, and Ph. Avouris, Phys. Rev. B **32**, 4296 (1985).
[55] J. P. Cowin, D. J. Auerbach, C. Becker, and L. Wharton, Surf. Sci. **78**, 545 (1978).